Design and Evaluation of a Zero Mass Flow Liner

Ralf Burgmayer*
German Aerospace Center (DLR), Institute of Propulsion Technology, Engine Acoustics, D-10623 Berlin, Germany

Friedrich Bake†
Bundesanstalt für Materialforschung und -prüfung (BAM), Department of Non-destructive Testing, Acoustic and Electromagnetic Methods, Unter den Eichen 87, D-12205 Berlin, Germany

Lars Enghardt‡
German Aerospace Center (DLR), Institute of Propulsion Technology, Engine Acoustics, D-10623 Berlin, Germany

In this study, the concept of a Zero Mass Flow Liner is evaluated. The concept enables impedance control by the induction of periodic bias flow through the perforated facing sheet of the liner. The periodic bias flow is generated by a secondary high amplitude acoustic actuation. By means of the periodic bias flow, the liner can be tuned to different operating points in a given range of grazing flow velocities. The equivalent fluid impedance model for perforated plates is modified to account for the effects of periodic bias flow and grazing flow. An optimization routine, based on a genetic algorithm, is implemented. The method is applicable to any liner concept and uses the impedance of the lined surface as boundary condition in a numerical simulation. Thereby, a set of liner parameters is derived in order to obtain the desired damping characteristics. Based on the results of the optimization, a Zero Mass Flow Liner is manufactured and consequently evaluated experimentally. The damping characteristics are evaluated in form of the dissipated energy along the lined surface. Prediction and measurements show agreement. The Zero Mass Flow Liner delivers broad band dissipation of high peak value over a range of grazing flow Mach numbers. Under grazing flow conditions, the effect of periodic bias flow is reduced. This poses high energy requirements in high Mach number flow regimes which might restrict the applicability of the Zero Mass Flow concept to grazing flows of low Mach numbers.

Nomenclature

c_0	Speed of sound in air
$C_{d,nl}$	Empirical discharge coefficient accounting for periodic bias flow effects
d	Orifice diameter
D_{cav}	Cavity depth
D	Length of perfectly matched layer (PML) in x-direction
f_p	Frequency of the primary excitation (sound field in the main duct)
f_s	Frequency of the secondary excitation (periodic bias flow)
h	Thickness of the perforated facing sheet

*Research Assosciate, DLR Institute of Propulsion Technology, Engine Acoustics, ralf.burgmayer@dlr.de.
†Head of the Division for Acoustic and Electromagnetic Methods, BAM, AIAA Senior Member, friedrich.bake@bam.de.
‡Professor, DLR Institute of Propulsion Technology, Engine Acoustics, AIAA Member, lars.enghardt@dlr.de.

k	Wave number of the primary excitation
L_{eff}	Effective length of the lined surface
l_{GF}	Change of end correction due grazing flow
l_s	Change of end correction due to periodic bias flow
M_{avg}	Average grazing flow mach number
p	Acoustic pressure of the primary excitation (sound field in the main duct)
p_s	Acoustic pressure of the secondary excitation (periodic bias flow)
r	Orifice radius
St_p	Periodic bias flow Strouhal number
u_s	Acoustic particle velocity in the orifices of the facing sheet, induced by the secondary actuation
v_{avg}	Average grazing flow speed
α_∞	Tortuosity
δ	Inertial end correction
ζ	Specific impedance of the perforated plate
ζ_{Cav}	Specific impedance of the cavity
ζ_{exit}	Specific impedance at the exit of the numerical domain
ζ_{ZML}	Specific impedance of the Zero Mass Flow Liner
$Re\{\Delta\zeta_s\}$	Resistance due to periodic bias flow
$Re\{\Delta\zeta_{GF}\}$	Resistance due to grazing flow
η	Dynamic viscosity
Λ	Hydraulic radius
ρ_0	Density of air
$\tilde{\rho}_e$	Effective density
σ	Flow resistivity
τ	Cost function
Φ	Porosity of the facing sheet
ψ	Correction for hole interaction
ω_p	Angular frequency of the primary excitation (sound field in the main duct)

I. Introduction

Increased noise regulations in aviation necessitate liner concepts with improved low frequency and broad band damping. In 2008, Heuwinkel et al.[1] presented the concept of a so-called Zero Mass Flow Liner, where an acoustic actuator is attached to the cavity of a Helmholtz resonator liner, emitting a secondary high amplitude sound field and thereby inducing periodic bias flow in the orifices of the facing sheet. Thereby, the net mass flow through the facing sheet of the liner is zero. Lahiri et al.[2] described the design of an aeroacoustic actuator as source for the excitation of periodic bias flow. This configuration requires some air supply, but reduces the mass flow rate by 60 % at similar performance when compared to a conventional steady bias flow liner. While demonstrating extended dissipation characteristics, dependent on the actuation strength, no quantitative analysis of the underlying physics has been conducted. Based on dimensional analysis, the effects of a secondary high amplitude stimulus on the impedance of a perforated plate at primary sound field frequencies have been analyzed experimentally. The secondary and primary stimuli were unrelated in terms of frequency and phase. Due to the secondary sound source, periodic bias flow is induced in the orifices of the perforated plate, resulting in a change of impedance. A semi empirical model describing the change of impedance is deduced from the measurements.[3,4] This manuscript describes the design process and the consecutive experimental evaluation of a Zero Mass Flow Liner. The process is decomposed into three steps: First, the equivalent fluid impedance model, derived by Atalla and Sgard,[5] is modified to account for the flow separation effects due to the secondary periodic bias flow and grazing flow.[3,4,6] Second, an optimization routine, based on a genetic algorithm,[7] is implemented. In the process, the two dimensional Helmholtz Equation is solved numerically. Thereby, the impedance calculated from the derived impedance model is used as boundary condition in the simulation, making the method applicable to arbitrary lined surfaces. A predefined dissipation characteristic serves as target function. The difference between the calculated dissipation and the target dissipation is minimized iteratively by the variation of the geometric parameters of the liner and the strength of the periodic bias flow. Using the parameters obtained in the optimization

This is the author's version (post-print) of the work that was accepted for publication in the proceedings of the 28th AIAA/CEAS Aeroacoustics Conference held in Southampton, United Kingdom, June 2022.
The final version was published in the proceedings of the conference as paper No. 2022-2820.
https://arc.aiaa.org/doi/abs/10.2514/6.2022-2820

process, a liner is manufactured. To maintain flexibility regarding the actuation frequency of the periodic bias flow, loudspeakers are used for excitation. Third, the manufactured Zero Mass Flow Liner is evaluated experimentally. The measured dissipation is compared to the results of the simulation up to grazing flows with an average Mach number of 0.2.

II. Zero Mass Flow Concept

Figure 1 depicts a schematic of the Zero Mass Flow Liner (ZML). An acoustic actuator is attached to the cavity of a Helmholtz resonator liner. In general, any form of acoustic source able to emit high amplitude signals can be used. E.g. Lahiri et al.[2] used an aeroacoustic actuator to excite the periodic bias flow. In this study, loudspeakers are used. Due to the high amplitude sound wave emitted by the actuator, periodic bias flow is induced in the orifices of the facing sheet, altering the impedance of the liner and consequently affecting its damping characteristics. The periodic bias flow, referred to as secondary flow, is quantified by the amplitude of the root mean squared (RMS) particle velocity in the orifices of the perforated facing sheet $|\bar{u}_s|$. By adjusting $|\bar{u}_s|$, the impedance of the lined surface can thus be adapted to specific operating conditions.

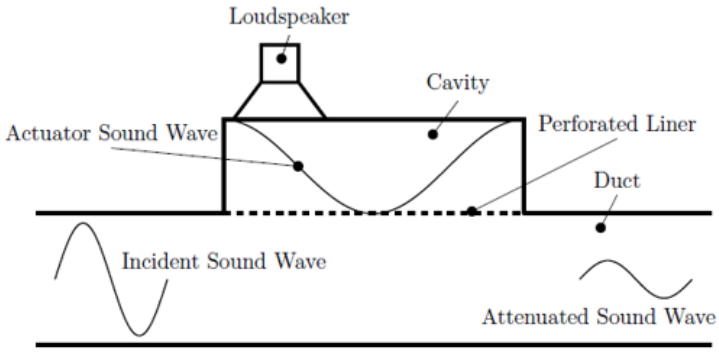

Figure 1. Schematic of a Zero Mass Flow Liner in a duct configuration.[1]

III. Impedance Model for the Zero Mass Flow Liner under Grazing Flow

Atalla and Sgard use the equivalent fluid approach to derive an impedance model for perforated plates.[5] The model can be applied to macro and micro perforated plates. Flow separation effects are not incorporated. Following Laly et al.,[8] this section describes the extension of the model to account for flow separation due to periodic bias and grazing flow. The specific impedance of the perforated plate is given by equation (1):

$$\zeta = j\frac{\omega_p h}{\rho_0 c_0 \Phi}\tilde{\rho}_e, \tag{1}$$

where h represents the plate thickness and $\omega_p = 2\pi f_p$ is the circular frequency. f_p is the frequency of the sound field excited in the main duct and referred to as primary sound field. ρ_0 and c_0 represent the density and speed of sound in air and Φ represents the porosity of the perforated plate. $\tilde{\rho}_e$ denotes the effective density given as:

$$\tilde{\rho}_e = \alpha_\infty \rho_0 \left(1 + \frac{\sigma\Phi}{j\omega\alpha_\infty\rho_0}\sqrt{1 + \frac{4j\rho_0\omega_p\eta\alpha_\infty^2}{\Phi^2\sigma^2\Lambda^2}}\right), \tag{2}$$

where η represents the dynamic viscosity of air and Λ the hydraulic radius of the orifices. In case of circular orifices, the hydraulic radius is equal to the orifice radius $\Lambda = r$. $\tilde{\rho}_e$ is a function of the flow resistivity σ and the tortuosity α_∞. σ is given by:

$$\sigma = \frac{8\eta}{\Phi r^2} \tag{3}$$

and α_∞ is defined as:

This is the author's version (post-print) of the work that was accepted for publication in the proceedings of the 28th AIAA/CEAS Aeroacoustics Conference held in Southampton, United Kingdom, June 2022.
The final version was published in the proceedings of the conference as paper No. 2022-2820.
https://arc.aiaa.org/doi/abs/10.2514/6.2022-2820

$$\alpha_\infty = 1 + \frac{2\delta\psi}{h}, \tag{4}$$

where $\delta = 0.48\sqrt{\pi r^2}$ represents the one-sided inertial end correction and ψ represents a function to account for the interaction of adjacent orifices. Here, for ψ, we use the derivation of Fok.[9]

High sound pressure amplitudes, bias and grazing flows introduce flow separation effects at the orifices of the perforated plate resulting in a change of impedance by altering α_∞ and σ. The change of resistance due to a high amplitude secondary sound wave, i.e. periodic bias flow is given as:

$$Re\{\Delta\zeta_s\} = \frac{(1-\Phi^2)|\bar{u}_s|}{2c_0\Phi C_{d,nl}^2} \cdot (1 - \frac{f_p d}{|\bar{u}_s|}), \tag{5}$$

The first term on the right hand side accounts for the increase in resistance under quasi-steady flow conditions, where $C_{d,nl}$ describes the discharge coefficient approximated empirically.[3] The second term on the right hand side accounts for deviations from the quasi-steady assumption in the transmission region between linear and quasi-steady flow domains. This correction term is derived from previous measurements in Appendix A. To account for flow separation effects due to grazing flow, the expression of Guess[6] is used:

$$Re\{\Delta\zeta_{GF}\} = \frac{(1-\Phi^2)}{\Phi} \cdot k \cdot M_{avg}, \tag{6}$$

where k is a measure for the turbulence intensity and is set to $k = 0.3$. M_{avg} depicts the grazing flow Mach number. Because σ can be viewed as the resistance per unit thickness, it is increased by the flow separation effects. Using Eqs. (5) and (6), the flow resistivity under periodic bias flow and grazing flow is expressed as:

$$\sigma_{fs} = \frac{8\eta}{\Phi r^2} + \rho_0 c_0 \frac{(Re\{\Delta\zeta_s\} + Re\{\Delta\zeta_{GF}\})}{h}, \tag{7}$$

where, in a first approximation, an additive relation between the convective terms is used.[10,11] The flow separation also affects the reactive part of the impedance. Fluid is transported away from the orifices, reducing the inertial end correction of the perforate and, hence, the tortuosity. The loss of end correction, induced by the secondary flow is accounted for by multiplying the end correction with the factor l_s:[4]

$$l_s = 0.38 + \frac{0.68}{1 + 1/St_{p,h}^2}, \tag{8}$$

where $St_{p,h} = \frac{2\pi f_p h}{|\bar{u}_s|}$ is the periodic bias flow Strouhal number based on the plate thickness. The loss of end correction due to grazing flow is accounted for by multiplying the end correction by the approximation of Guess:[6]

$$l_{GF} = \frac{1}{1 + 305 M_{avg}^3}. \tag{9}$$

Consequently, the tortuosity in case of periodic bias flow and grazing flow is rewritten as:

$$\alpha_{\infty,fs} = 1 + \frac{2\delta\psi}{h} \cdot l_s \cdot l_{GF}. \tag{10}$$

The cavity is, under the assumption of a rigid back wall and the sole propagation of plane waves, modelled using the common expression $\zeta_{Cav} = -j\cot(\omega_p D_{cav}/c_0)$, where D_{cav} is the cavity depth. Thus, the impedance of the ZML under secondary actuation and grazing flow is written:

$$\zeta_{ZML} = j\frac{\omega h}{\rho_0 c_0 \Phi}\tilde{\rho}_{e,fs} - j\cot(\omega_p D_{cav}/c_0), \tag{11}$$

where $\tilde{\rho}_{e,fs}$ is the effective density accounting for flow separation effects. The effects of high amplitude primary sound fields on the impedance can be neglected if the particle velocity in the orifices due to the secondary excitation is larger than the orifice velocity induced by the primary excitation.[3]

This is the author's version (post-print) of the work that was accepted for publication in the proceedings of the 28th AIAA/CEAS Aeroacoustics Conference held in Southampton, United Kingdom, June 2022.
The final version was published in the proceedings of the conference as paper No. 2022-2820.
https://arc.aiaa.org/doi/abs/10.2514/6.2022-2820

IV. Optimization, Numerical Method, Liner Design and Manufacturing

A. Optimization method and assumptions

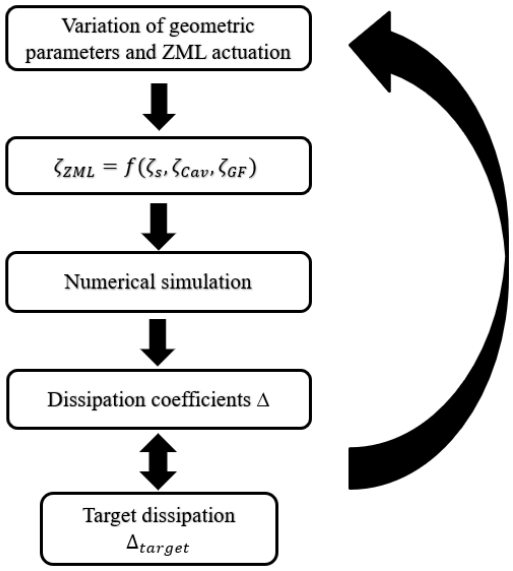

Figure 2. Flow diagram of the optimization routine.

Fig. 2 depicts a flow chart outlining the optimization process. The optimization scheme is only applied to the case of upstream excitation. For downstream excitation a separate optimization is necessary. The impedance of the ZML, calculated via Eq. 11 is used as boundary condition in the numeric calculations, described in Sec. B. Thereby, the sound propagation, restricted to plane waves, is calculated in the duct. By a consecutive plane wave decomposition, the scattering coefficients and the dissipation along the lined section of the duct are calculated. The frequency range considered is 204 Hz $\geq f_p \leq$ 1989 Hz. This corresponds to the frequency range considered in the experimental part of the study. For the optimization, a genetic optimization algorithm is used.[7] The optimization procedure is based on the iterative minimization of a cost function τ:

$$\tau = 1 - \frac{1}{f_{p,2} - f_{p,1}} \int_{f_{p,1}}^{f_{p,2}} \Delta^{+} df_p, \tag{12}$$

where $f_{p,1}$ and $f_{p,2}$ denote the lower and upper cut-off frequencies. $f_{p,1}$ is set to $f_{p,1} = 408$ Hz and $f_{p,2}$ is set to $f_{p,2} = 1734$ Hz respectively. In each optimization step, prior to a recalculation of the sound pressure distribution in the duct, the impedance of the ZML is varied by changing the geometric parameters of the facing sheet (hole diameter d, plate thickness h and porosity Φ) and $|\bar{u}_s|$ until τ is minimized. The depth of the cavity is set to a fixed value of $D_{cav} = 60$ mm to enable the estimation of the particle velocity in the cavity by a plane wave decomposition during the experimental evaluation. Note, that the cavity depth is the parameter that mainly defines the resonance frequency of the liner.

The optimization is conducted in two steps. First, an optimization is conducted at $M_{avg} = 0$ to derive a set of geometric parameters and the required acoustically induced periodic bias flow velocity in the orifices of the facing sheet $|\bar{u}_{s,opt}|$. Both, grazing flow and periodic bias flow cause flow separation at the facing sheet of the liner. As a consequence, the real part of the impedance (resistance) increases while the imaginary part (reactance) decreases. Thus, the required $|\bar{u}_s|$ will decrease with increasing grazing flow speeds. Therefore, in a second step, the derived geometric parameters are used to minimize the target function at $|\bar{u}_s| = 0$ under variation of the grazing flow speed, to find the maximum M_{avg} up to which the optimum dissipation, defined by the target function, can be maintained. By adjusting $|\bar{u}_s|$ accordingly, a high degree of dissipation should be provided for $0 \leq M_{avg} \leq M_{avg,opt}$. The geometric parameters obtained from the optimization are

This is the author's version (post-print) of the work that was accepted for publication in the proceedings of the 28th AIAA/CEAS Aeroacoustics Conference held in Southampton, United Kingdom, June 2022.
The final version was published in the proceedings of the conference as paper No. 2022-2820.
https://arc.aiaa.org/doi/abs/10.2514/6.2022-2820

consequently used to manufacture a facing sheet for the liner. The optimized set of parameters is summarized in table 1.

Table 1. Parameters of the optimized facing sheet.

$M_{avg,opt}$	d [mm]	h [mm]	Φ [%]	$\lvert\bar{u}_{s,opt}\rvert$ [m/s]
0.14	1.62	1.04	4.94	14.31

Certain assumptions are made with respect to the process of optimization. The sound pressure amplitude in the main duct is negligible under either periodic bias flow actuation or grazing flow. The former is assumed under the premise that the amplitude of the periodic bias flow is larger than the sound pressure amplitude in the main duct.[3] The latter is verified empirically for a sound pressure level of 130 dB in the main duct. For $M_{avg} \geq 0.1$ the effect is found to be negligible. The propagation of sound in sections 1 and 2 of the computational domain (see Fig. 5) is restricted to plane waves. Under certain circumstances, the impedance expresses a dependency on the secondary actuation frequency f_s.[3] The dependency of the impedance on f_s is neglected. The cavity back wall of the liner is assumed to be rigid, despite the attached acoustic actuator. Certain limiting values have been set to keep the geometric parameters of the facing sheets in the range of values, the semi empirical model was derived in and verified for. Furthermore, achievable values must be maintained with regards to practicability. An example is the combination of the actuator particle velocity $|\bar{u}_s|$ and the porosity of the facing sheet Φ. The change of resistance due to the periodic bias flow actuation is a function of $|\bar{u}_s|$ (see Eq. (5)). As $|\bar{u}_s|$ is a function of Φ (see Eq. (21)), in order to achieve sufficiently high $|\bar{u}_s|$ for facing sheets of high porosities, high sound pressure amplitudes are necessary, that may not be achieved practically or only with great effort, respectively. The limits, imposed on the optimization process, are listed in table 2.

Table 2. Limiting values for the variation of parameters in the optimization.

Parameter	min	max
$\lvert\bar{u}_s\rvert$ [m/s]	0	15
d [mm]	1	2.5
h [mm]	1	2
d/h	0.75	2.5
Φ [%]	1	6

Figures 3 a) and b) depict the optimized specific impedances and the resulting dissipation for upstream excitation for the cases of no grazing flow and no periodic bias flow. In both cases, the optimized ζ_{ZML} takes a value near 1 and the resulting dissipation is of broad band character. For the case of grazing flow, the optimized impedance is of lower resistance and the reactance exhibits an increased loss of end correction. Because of the lower resistance, the dissipation is of slightly lesser bandwidth and exhibits an increased peak value. Due to the lower reactance in the case of grazing flow, the resonance frequency is shifted slightly to higher frequencies.

B. Numerical method

This section outlines the numerical method utilized in the optimization. The propagation of sound under mean flow in a two dimensional channel with a section of perforated wall, similar to Fig. 4, is calculated by solving the two dimensional convected Helmholtz equation (2DCHE) for a harmonic perturbation of the acoustic pressure $\tilde{p}$. The 2DCHE is solved by means of the finite difference method. Further details of the numerical procedure can be found in Weng et al.[12] The two dimensional convected Helmholtz equation is given by:

$$(1 - M_{avg}^2)\frac{\partial^2 \tilde{p}}{x^2} + \frac{\partial^2 \tilde{p}}{y^2} - 2jkM_{avg}\frac{\partial \tilde{p}}{x} + k^2\tilde{p} = 0, \tag{13}$$

where $k = \omega_p/c_0 = 2\pi f_p/c_0$ is the wave number. The boundary condition on the hard wall is given by:

This is the author's version (post-print) of the work that was accepted for publication in the proceedings of the 28th AIAA/CEAS Aeroacoustics Conference held in Southampton, United Kingdom, June 2022.
The final version was published in the proceedings of the conference as paper No. 2022-2820.
https://arc.aiaa.org/doi/abs/10.2514/6.2022-2820

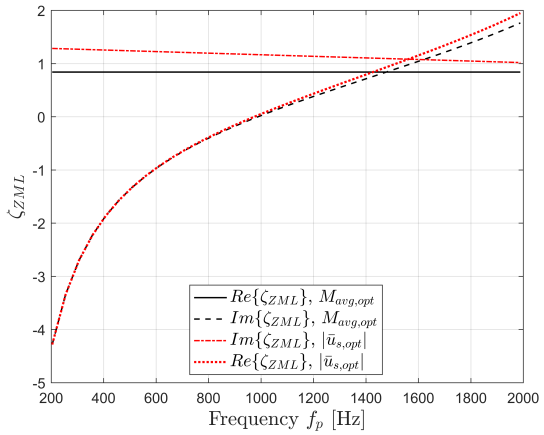

(a) Predicted specific impedance ζ_{ZML}.

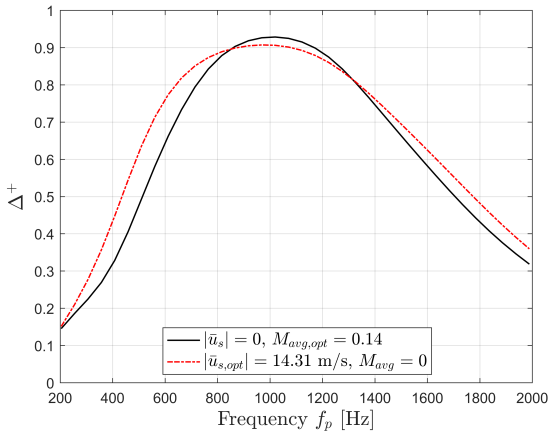

(b) Predicted dissipation for upstream excitation Δ^+.

Figure 3. Results of the optimization.

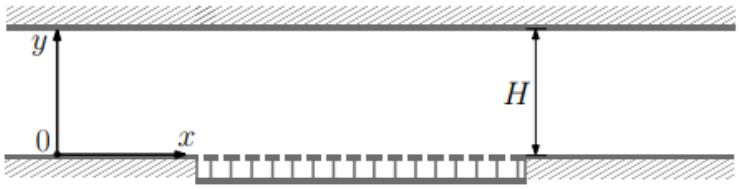

Figure 4. Two dimensional channel with a perforated wall.

$$\frac{\partial \tilde{p}}{\partial y} = 0. \tag{14}$$

The boundary condition on the perforated wall is given by the Ingard-Myers conditions, where the specific impedance of the ZML ζ_{ZML} from Eq. (11) is applied as specific wall impedance:

$$\left[\frac{jk}{\zeta_{ZML}} + \frac{2M_{avg}}{\zeta_{ZML}}\frac{\partial}{\partial x} - \frac{jM_{avg}^2}{k\zeta_{ZML}}\frac{\partial^2}{\partial x^2}\right]\tilde{p} - \frac{\partial \tilde{p}}{\partial y} = 0. \tag{15}$$

At the inlet plane, a pressure profile is prescribed as boundary condition. Given that only plane waves propagate, the boundary condition at the exit of the numerical domain is of the form:[13]

$$\frac{jk\tilde{p}}{M_{avg} + \zeta_{exit}} + \frac{\tilde{p}}{\partial x}, \tag{16}$$

where ζ_{exit} represents the specific impedance at the exit of the numerical domain. ζ_{exit} is set to $\zeta_{exit} = 1$. In addition, an anechoic condition in form of a perfectly matched layer (PML) is imposed on the outlet plane.[14,15] Fig. 5 displays the computational domain with an exemplary mesh. The domain is divided in three sections: Sections 1 and 3 represent the hard walled channel sections, while section 2 contains the lined segment with $\zeta = \zeta_{ZML}$ as the south wall. The north wall of section 2 is defined as hard wall respectively. Sections 1 and 3 are of length 0.9 m, while the lined section is of length 0.204 m. This corresponds to the effective length L_{eff} of the subsequently manufactured ZML. $y = 60$ mm corresponds to the height above the lined surface H and is adapted from the DLR flow channel DUCT-R, which is described in Sec. V A. The length of the PML in x-direction D is dynamic and always corresponds to half of the wave length of the frequency of the pressure perturbation that is calculated $D = 0.5\lambda_p$. 2-D Gauss-Lobatto grid points are applied in each section for the mesh generation. At the interfaces between adjacent sections the continuity of $\tilde{p}$ and $\frac{\partial \tilde{p}}{\partial x}$ is applied. The number of grid points is increased at the transitions from hard wall to lined section and vice versa. A convergence analysis is performed to determine a sufficient number of grid points.

This is the author's version (post-print) of the work that was accepted for publication in the proceedings of the 28th AIAA/CEAS Aeroacoustics Conference held in Southampton, United Kingdom, June 2022.
The final version was published in the proceedings of the conference as paper No. 2022-2820.
https://arc.aiaa.org/doi/abs/10.2514/6.2022-2820

Once the pressure distribution in the channel is calculated, the pressure values at several x-coordinates in sections 1 and 3 are used to decompose the wave field into incident and reflected plane waves at the lined surface. Thermo-viscous effects are neglected in the pressure calculations but incorporated in the plane wave decomposition. Subsequently, the scattering coefficients are derived and the dissipation $\Delta^{\pm}$ for upstream and downstream excitation is calculated. The decomposition method and the calculation of the scattering coefficients and $\Delta^{\pm}$ is similar to the procedure used in the experimental evaluation, see Sec. V B.

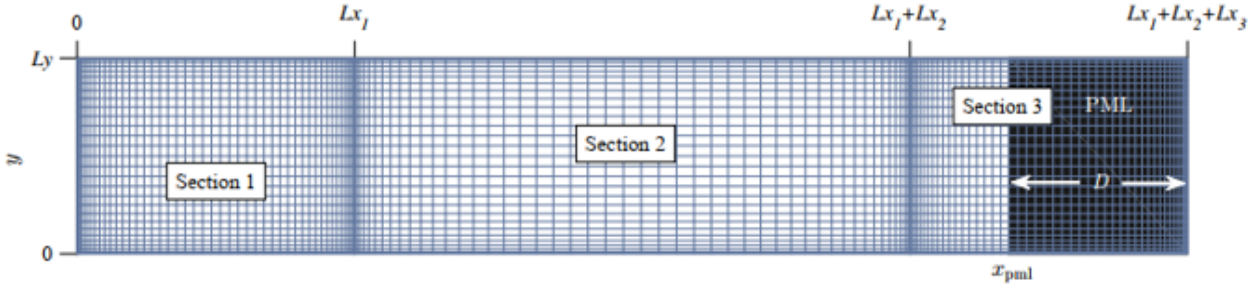

Figure 5. Meshed computational domain.

C. Liner Design and Manufacturing

The facing sheet and the liner body are manufactured from aluminum. The liner features an overall length of 220 mm. The back wall is of thickness 7 mm and the side walls are of thickness 4 mm. The cavity is divided into three identical chambers of size 68 mm x 72 mm x 60 mm, divided by walls of thickness 4 mm. The effective length of the liner is therefore approximately $L_{eff} = 204$ mm. Each chamber is equipped with an inlet for the induction of periodic bias flow and two chambers are equipped with several flush mounted microphones each, to allow an estimation of the induced particle velocity via a plane wave decomposition. Figs. 6 a) and b) show the CAD model of the liner body and the manufactured ZML installed in DUCT-R respectively. The periodic bias flow is excited by speakers, one connected to each cavity chamber via a tubing system with a diameter of 10 mm. Hence, the inlets are small compared to the area of the cavity back wall. Nevertheless, the inlets cause derivations from a rigid cavity by introducing additional resonances. The tubing system, connecting the speakers to the cavity chambers, is of length 250 mm. Loudspeakers serve as actuators in order to retain maximum flexibility regarding the actuation frequency. The facing sheet was manufactured with a slightly higher porosity of $\phi = 5.17$ %. This difference arises due to the fact, that the orifices have to be distributed homogeneously over the sub areas of the chambers without placing parts of the orifices above the separating walls of the chambers or reducing the effective, perforated area of the liner.

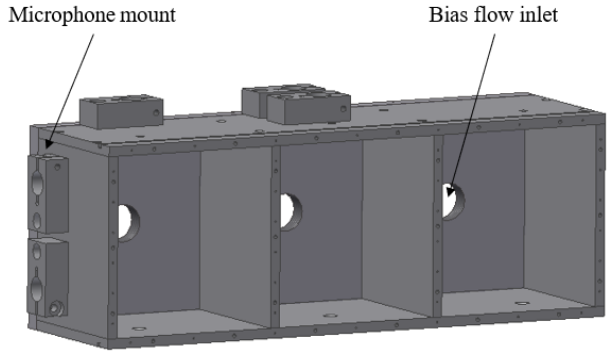

(a) CAD of ZML body.

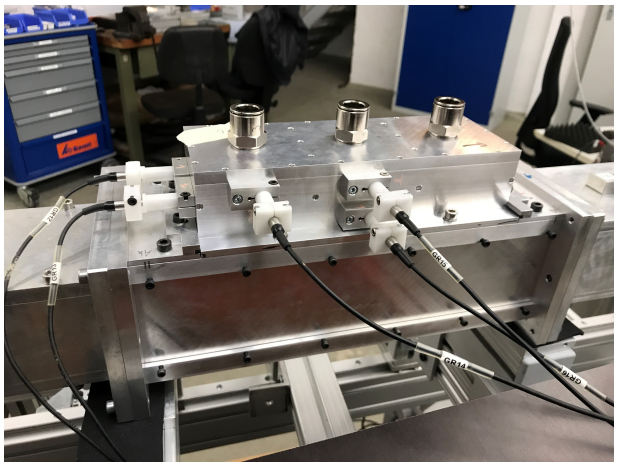

(b) ZML installed in DLR flow duct facility DUCT-R.

Figure 6. Designed and manufactured ZML.

This is the author's version (post-print) of the work that was accepted for publication in the proceedings of the 28th AIAA/CEAS Aeroacoustics Conference held in Southampton, United Kingdom, June 2022.
The final version was published in the proceedings of the conference as paper No. 2022-2820.
https://arc.aiaa.org/doi/abs/10.2514/6.2022-2820

V. Experimental Setup and Analysis Method

A. Experimental Setup

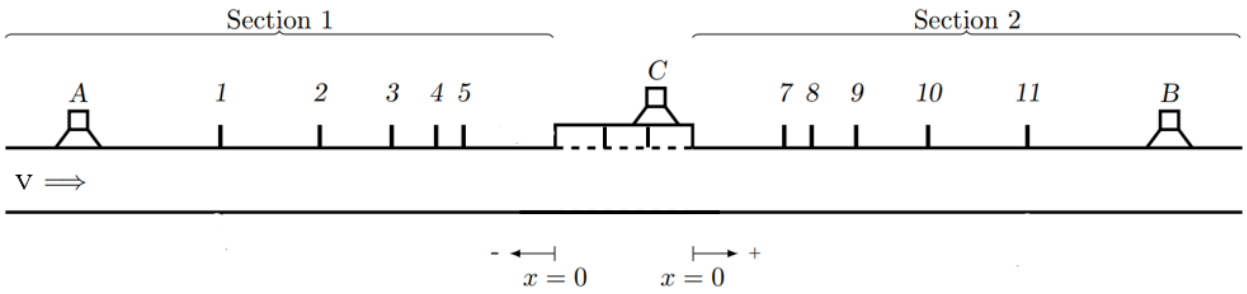

Figure 7. Experimental Setup.

Fig. 7 depicts the experimental setup. The ZML is mounted between the two duct sections of the flow duct facility DUCT-R of the German Aerospace Center (DLR), Berlin. The rectangular duct is of width 80 mm and height 60 mm and features plane wave excitation up to approximately 2150 Hz. Grazing flow can be applied via section 1, allowing for grazing flow speeds up to $M_{avg} \approx 0.25$. Each section is equipped with an anechoic termination. The sound field in the duct is, in the form of single tone stimuli, alternately excited by loudspeakers LS A and LS B in the frequency range $204 \leq f_p \leq 1989$ Hz, allowing for a wave decomposition independent of end reflections.[16] The sound pressure level is defined in terms of the RMS level of the plane wave incident on the measurement section at $x = 0$ and was set to $\bar{p}_i = 130$ dB for all frequencies f_p. The influence of the sound pressure level in the duct on the impedance of the ZML is found to be negligible for the case of bias flow actuation or grazing flow with $M_{avg} \geq 0.1$. Each section is equipped with five logarithmically spaced microphones to capture the sound field in the duct. The secondary stimulus for the actuation of periodic bias flow is actuated by three speakers, one for each chamber of the cavity. This is depicted in Fig. 7 as a single speaker LS C respectively. The speakers are connected to the same signal generator in parallel, so phase differences between the speakers are assumed to be small. The secondary stimulus, inducing the periodic bias flow, is a pure sine tone. Harmonics are neglected due to their minor influence compared to the fundamental.[3] During the experimental program, we found $|\bar{u}_s|$ to vary slightly between the respective chambers of the liner due to the individual transfer functions of the speakers. Furthermore, with increasing operating time, the sound pressure radiated from the speakers, actuating the secondary flow, declined. Hence, additional variation of $|\bar{u}_s|$ over the measurement points is introduced. The measurement program was conducted in intervals to limit the variations of $|\bar{u}_s|$. The respective values of $|\bar{u}_s|$ listed in Sec. VI represent values averaged over the chambers and measurement points. The actuation frequency of the secondary stimulus f_s is chosen in a way, that the transmission efficiency through the tubing systems is maximum and plane wave propagation is ensured. f_s is found to be $f_s = 1235$ Hz for the given setup by exciting the cavity chambers simultaneously with a sweep signal.

B. Analysis Method

The primary sound field in the duct is excited alternately with speakers LS A and LS B and the microphone data in the duct is analyzed separately in sections 1 and 2. This results in four equations for the complex sound pressure in the duct:

$$\hat{p}_{1,a}(x) = \hat{p}^+_{1,a} e^{-ik_1^+ x} + \hat{p}^-_{1,a} e^{ik_1^- x}, \tag{17a}$$

$$\hat{p}_{2,a}(x) = \hat{p}^+_{2,a} e^{-ik_1^+ x} + \hat{p}^-_{2,a} e^{ik_1^- x}, \tag{17b}$$

$$\hat{p}_{1,b}(x) = \hat{p}^+_{1,b} e^{-ik_1^+ x} + \hat{p}^-_{1,b} e^{ik_1^- x}, \tag{17c}$$

$$\hat{p}_{2,b}(x) = \hat{p}^+_{2,b} e^{-ik_1^+ x} + \hat{p}^-_{2,b} e^{ik_1^- x}. \tag{17d}$$

$\hat{p}^+$ and $\hat{p}^-$ are the complex amplitudes of the upstream and downstream propagating waves. The subscripts denote the duct section and excitation with LS A or LS B respectively. The recorded signals are

This is the author's version (post-print) of the work that was accepted for publication in the proceedings of the 28th AIAA/CEAS Aeroacoustics Conference held in Southampton, United Kingdom, June 2022.
The final version was published in the proceedings of the conference as paper No. 2022-2820.
https://arc.aiaa.org/doi/abs/10.2514/6.2022-2820

transformed into the frequency domain by applying Chung's method to reject uncorrelated flow noise.[17] To derive the complex pressure amplitudes, Eqs. (17a) to (17d) are fitted to the microphone data. Thermo-viscous losses at the wall are incorporated in the wave number k by the solution of Dokumaci.[18] Consequently, the complex sound pressure amplitudes at $x = 0$ are identified. The sound pressure amplitudes are related to each other via the scattering coefficients r and t of the lined surface. r is the reflection coefficient, describing the reflected part of the sound wave at the transition from rigid to lined wall, and t is the transmission coefficient. Figure 8 depicts the sound field in the duct for excitation with LS A and LS B. r and t are calculated by combining both measurements and rewriting Eqs. (17a) to (17d):

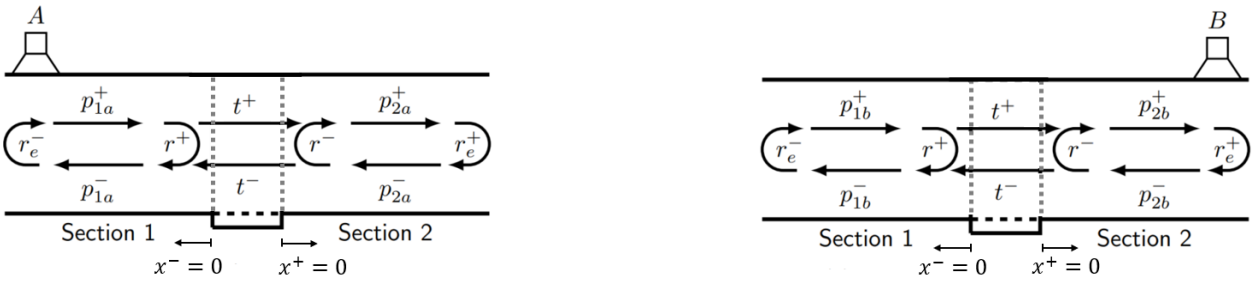

(a) Upstream excitation, measurement A.

(b) Downstream excitation, measurement B.

Figure 8. Sound field in the duct for upstream and downstream excitation.

$$r^+ = \frac{\hat{p}^-_{1,a}\hat{p}^-_{2,b} - \hat{p}^-_{1,b}\hat{p}^-_{2,a}}{\hat{p}^+_{1,a}\hat{p}^-_{2,b} - \hat{p}^+_{1,b}\hat{p}^-_{2,a}}; \qquad r^- = \frac{\hat{p}^+_{1,a}\hat{p}^+_{2,b} - \hat{p}^+_{1,b}\hat{p}^+_{2,a}}{\hat{p}^+_{1,a}\hat{p}^-_{2,b} - \hat{p}^+_{1,b}\hat{p}^-_{2,a}}; \tag{18}$$

$$t^+ = \frac{\hat{p}^+_{2,a}\hat{p}^-_{2,b} - \hat{p}^+_{2,b}\hat{p}^-_{2,a}}{\hat{p}^+_{1,a}\hat{p}^-_{2,b} - \hat{p}^+_{1,b}\hat{p}^-_{2,a}}; \qquad t^- = \frac{\hat{p}^+_{1,a}\hat{p}^-_{1,b} - \hat{p}^+_{1,b}\hat{p}^-_{1,a}}{\hat{p}^+_{1,a}\hat{p}^-_{2,b} - \hat{p}^+_{1,b}\hat{p}^-_{2,a}}. \tag{19}$$

From the scattering coefficients, the dissipation Δ is calculated. Δ is a measure of the sound energy dissipated along the lined surface. Δ^+ represents the dissipation in case of upstream sound excitation (LS A) and Δ^- represents the dissipation in case of downstream excitation (LS B).

$$\Delta^\pm = 1 - \left(\frac{(1 \mp M_{avg})^2}{(1 \pm M_{avg})^2} \cdot |r^\pm|^2 + |t^\pm|^2 \right). \tag{20}$$

To estimate $|\bar{u}_s|$, the sound field in the cavity, actuated by LS C, is also decomposed into incident and reflected waves, similar to the process described above. Note, that due to the low microphone spacing in the cavity, the plane wave decomposition should be considered an estimate. From the plane wave components in the cavity, $|\bar{u}_s|$ is calculated from Euler's equation under the assumption of continuity:

$$|\bar{u}_s| = \frac{|\hat{p}^+_{s,cav} - \hat{p}^-_{s,cav}|}{\rho_0 c_0 \Phi \sqrt{2}}, \tag{21}$$

where $\hat{p}^+_{s,cav}$ describes the incident plane wave component at the facing sheet and $\hat{p}^-_{s,cav}$ describes the reflected component respectively.

VI. Results

A. Experimental Evaluation of the Optimization Process

Figure 9(a) depicts the measured dissipation coefficients compared to the dissipation obtained in the optimization process for the case $|\bar{u}_{s,opt}|$, $M_{avg} = 0$. Compared to the optimized value $|\bar{u}_{s,opt}| = 14.31$ m/s, the measured particle velocity of the periodic bias flow, averaged over all chambers and measurement points, is $|\bar{u}_s| \approx 13.48$ m/s. Slight disagreement is found for $600 \geq f_p \leq 1400$ Hz due to the additional cavity resonances induced by the bias flow supply. These deviations are a consequence of the assumption of a rigid cavity back wall and can be observed in all measurement results. The effects are found to decline with an

This is the author's version (post-print) of the work that was accepted for publication in the proceedings of the 28th AIAA/CEAS Aeroacoustics Conference held in Southampton, United Kingdom, June 2022.
The final version was published in the proceedings of the conference as paper No. 2022-2820.
https://arc.aiaa.org/doi/abs/10.2514/6.2022-2820

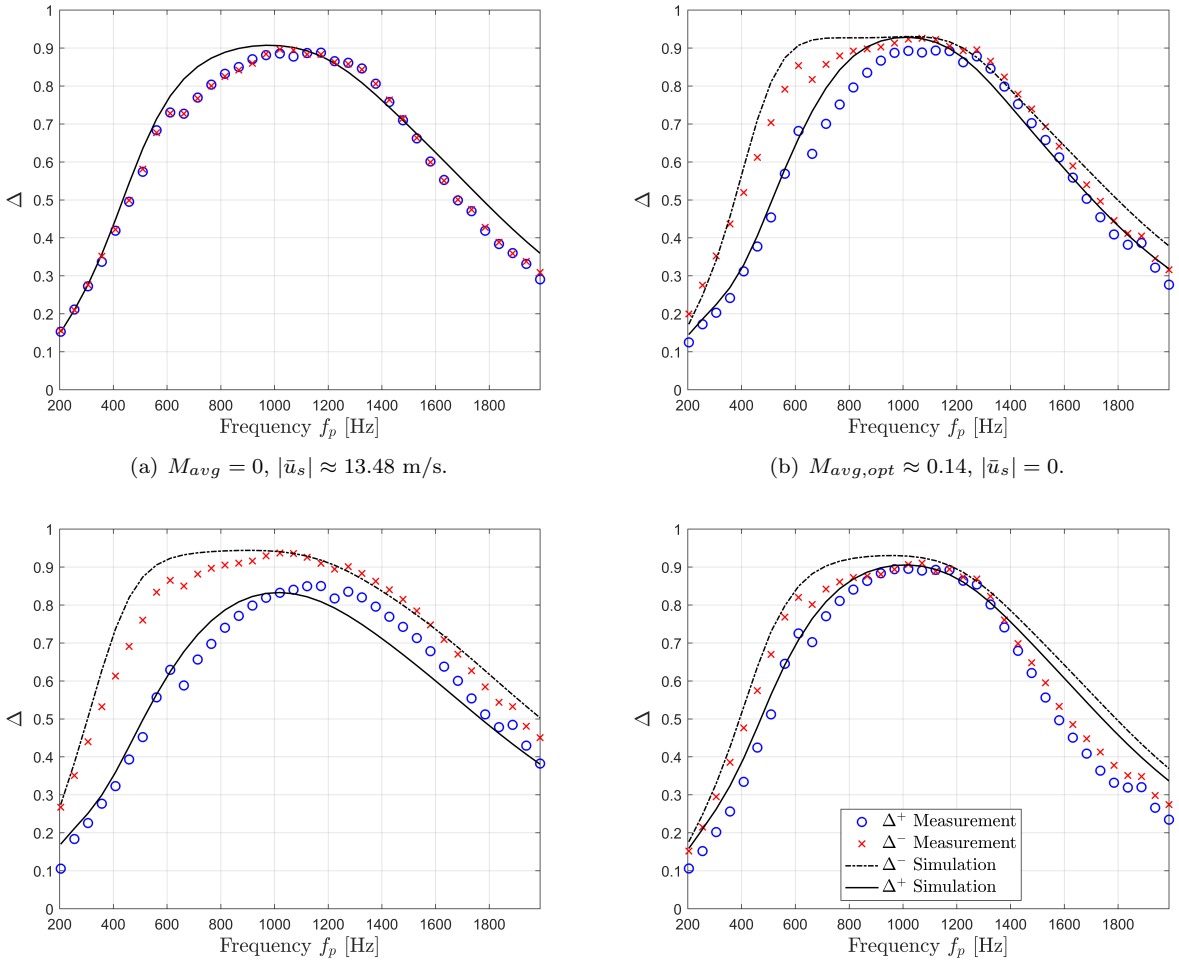

(a) $M_{avg} = 0$, $|\bar{u}_s| \approx 13.48$ m/s.

(b) $M_{avg,opt} \approx 0.14$, $|\bar{u}_s| = 0$.

(c) $M_{avg} \approx 0.19$, $|\bar{u}_s| = 0$.

(d) $M_{avg} \approx 0.08$, $|\bar{u}_s| \approx 8.53$ m/s.

Figure 9. Measured dissipation compared to results from the optimization process.

increasing resistance, i.e. for increased flow separation effects. For $f_p \geq 1500$ Hz some minor disagreement is observed as well. The deviations are assumed to be connected to the previously mentioned decline of $|\bar{u}_s|$ with increasing measurement time. Compared to a single degree of freedom liner, a significantly broadened dissipation is obtained. For $600 \geq f_p \leq 1500$ Hz the dissipation is larger than 0.7. The peak dissipation is approximately 0.9.

Figure 9(b) depicts the measured dissipation coefficients for upstream and downstream excitation compared to the dissipation obtained in the optimization process for the case $|\bar{u}_s| = 0$, $M_{avg,opt} = 0.14$. Measurement and optimization again show favorable agreement. As expected from the results of the optimization, the dissipation expresses slightly less broadband character and a slightly higher peak value compared to the case of periodic bias flow actuation. Additionally the results from a simulation for downstream excitation are plotted. For downstream excitation, simulation and measurement also obtain good agreement. Compared to the case of upstream excitation, the broad band character is increased further.

Figure 9(c) shows the comparison of the measured and simulated dissipation for $M_{avg} = 0.19$ and $|\bar{u}_s = 0|$. Good agreement between measurement and prediction is achieved. The prediction underestimates the resonance frequency slightly. Possibly, the loss of end correction due to grazing flow is underestimated by the model. Compared to the case $M_{avg} = 0.14$, the broadband dissipation is increased while the peak dissipation is decreased because of the risen resistance. For the case of upstream excitation, the resistance increased above its respective optimum, but the dissipation performance is still acceptable. For the case of downstream excitation, the obtained dissipation is of high peak and large bandwidth, emphasizing that

This is the author's version (post-print) of the work that was accepted for publication in the proceedings of the 28th AIAA/CEAS Aeroacoustics Conference held in Southampton, United Kingdom, June 2022.
The final version was published in the proceedings of the conference as paper No. 2022-2820.
https://arc.aiaa.org/doi/abs/10.2514/6.2022-2820

optimization needs to be conducted for upstream and downstream excitation separately.

For a decrease of grazing flow below its optimum value, in order to maintain a high degree of dissipation, the decrease of resistance is compensated by the actuation of periodic bias flow. Figure 9(d) displays the measured dissipation for $M_{avg} = 0.08$ and $|\bar{u}_{s,opt}| = 8.6$ m/s to the results of the simulation. Thereby, the necessary $|\bar{u}_s|$ is found by conducting the optimization for $M_{avg} = 0.08$ with fixed geometrical parameters. The measured secondary particle velocity is $|\bar{u}_s| \approx 8.53$ m/s. Compared to the case of only periodic bias flow or only grazing flow, measurement and prediction express larger discrepancies for $f_p \geq 1400$ Hz for both upstream and downstream excitation. The model overestimates the dissipation at high f_p. Compared to a single degree of freedom liner, a broad band dissipation of high peak value is achieved for upstream and downstream excitation.

B. Combined periodic bias and grazing flow

The grazing flow is found to suppress the periodic flow through the orifice. Consequently, the amplitude of the periodic bias flow is reduced with increasing grazing flow speeds. This is similar to the effect of a high amplitude primary sound field on the periodic bias flow.[3] Fig. 10(a) to 10(c) compare the measured dissipation for various grazing flow conditions with and without periodic bias flow actuation. Thereby, the ratio $\frac{v_{avg}}{|\bar{u}_s|}$, where v_{avg} is the average grazing flow speed, is increased from $\frac{v_{avg}}{|\bar{u}_s|} \approx 2.23$ to $\frac{v_{avg}}{|\bar{u}_s|} \approx 8.99$. For a ratio of $\frac{v_{avg}}{|\bar{u}_s|} \approx 2.23$ ($M_{avg} \approx 0.08$, $|\bar{u}_s| \approx 12.27$ m/s), the effect of the secondary actuation is clearly visible. Increasing $\frac{v_{avg}}{|\bar{u}_s|}$ leads to a reduced effect of the periodic bias flow. For $\frac{v_{avg}}{|\bar{u}_s|} \approx 5.1$ ($M_{avg} \approx 0.14$, $|\bar{u}_s| \approx 9.33$ m/s), the effect of the periodic bias flow on the dissipation is reduced considerably. For $\frac{v_{avg}}{|\bar{u}_s|} \approx 8.99$ ($M_{avg,max} = 0.19$, $|\bar{u}_s| \approx 7.3$ m/s), only a minor effect due to periodic bias flow around the resonance frequency of the liner is obtained. Thus, we assume the impedance of the lined surface is only negligibly affected by the periodic bias flow. The effect of high sound pressure levels on orifices and lined surfaces in grazing flows has been studied previously.[19–21] Thereby, the skin friction velocity v^* is compared to the acoustic particle velocity in the orifice $|u_0|$. As soon as v^* is in the order of the acoustic particle velocity in the orifices, the impedance change due to the high acoustic amplitudes is reduced. Goldman and Panton[19] for example, compare v^*, measured on a rigid wall part of the duct, to $|u_0|$ and find that effects due to high sound pressure amplitudes on the impedance of orifices are found only for $\frac{|u_0|}{v^*} > 3$. While determining v^* is out of scope of this study, previously measured data from DUCT-R is used for a comparison.[22] For $M_{avg} = 0.2$, v^* is found to be $v^* \approx 2.74$. Hence, the case $\frac{v_{avg}}{|\bar{u}_s|} \approx 8.99$ corresponds to $\frac{\sqrt{2}|\bar{u}_s|}{v^*} \approx 3.77$, agreeing to the values found in the literature.

C. Discussion of the Results

The results demonstrate, that the optimization routine can be used in the design of acoustic liners. The predicted dissipation of the Zero Mass Flow Liner, derived from the proposed impedance model in combination with the optimization method, agrees to the measurement results. Since the cavity was modelled under the assumption of a rigid back wall, minor deviations between prediction and measured dissipation arise due to additional cavity resonances introduced by the bias flow inlets. The accuracy of the impedance model of the Zero Mass Flow Liner can be increased by incorporating the actual impedance of the cavity. Dependent on the properties of the actuation supply, the impedance of the cavity might be difficult to derive analytically and needs to be measured beforehand. Therefore, a rigid cavity back wall was assumed in the process. The designed Zero Mass Flow Liner obtains broadband dissipation of high peak level for a grazing flow regime of $0 \geq M_{avg} \leq 0.2$ by inducing flow separation at the facing sheet of the liner and actively affecting its impedance. Utilizing multiple cavities of different depths, a high degree of broadband damping could be achieved. In principle, a liner can be designed to function over a range of desired grazing flow speeds. The liner should be designed in a way that, at the highest flow speed of consideration, no periodic bias flow is necessary. The decrease of resistance with decreasing grazing flow Mach number at differing operating conditions, can be compensated by applying the periodic bias flow actuation. With increasing grazing flow speeds however, the effect of the periodic bias flow gets suppressed. Hence, for high Mach numbers, a considerable amount of energy is necessary to achieve the desired effect. Take for example a Zero Mass Flow Liner that is designed to have a specific resistance of $Re\{\zeta\} \approx 1$ at $M_{avg} = 0.5$ without periodic bias flow actuation active. By neglecting the viscous contributions to the resistance as well as the radiation resistance, a porosity of $\Phi \approx 14.7$ % (see Eq. (6)) is required. Assuming one wants to utilize the effect of periodic bias

This is the author's version (post-print) of the work that was accepted for publication in the proceedings of the 28th AIAA/CEAS Aeroacoustics Conference held in Southampton, United Kingdom, June 2022.
The final version was published in the proceedings of the conference as paper No. 2022-2820.
https://arc.aiaa.org/doi/abs/10.2514/6.2022-2820

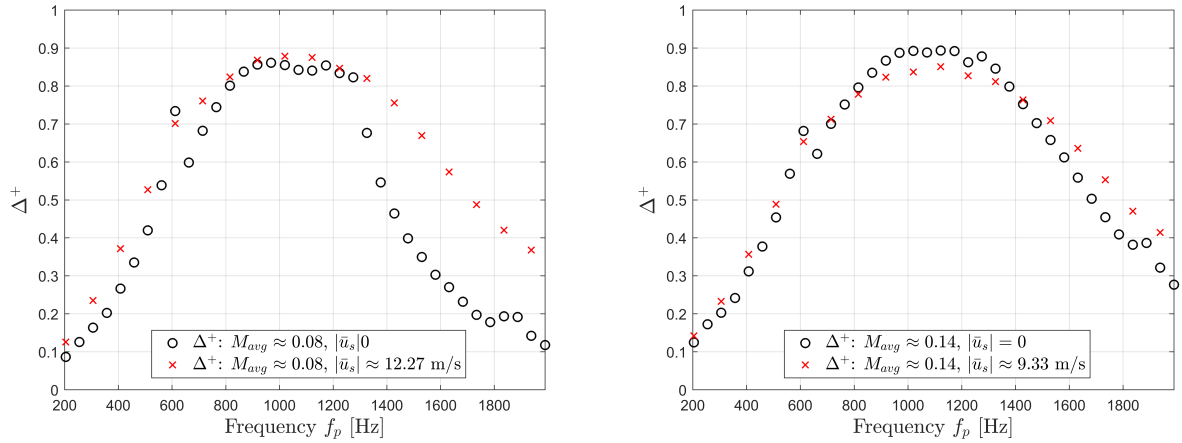

(a) $\frac{v_{avg}}{|\bar{u}_s|} \approx 2.23$. (b) $\frac{v_{avg}}{|\bar{u}_s|} \approx 5.1$.

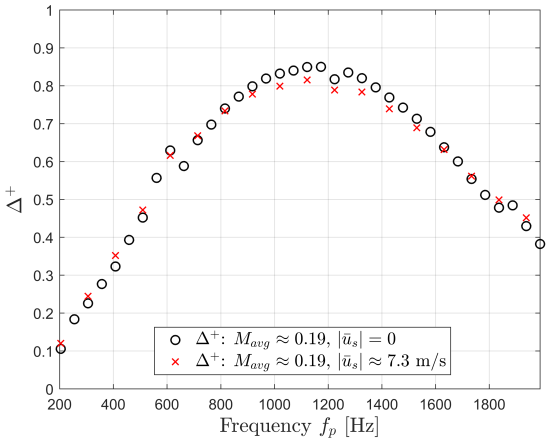

(c) $\frac{v_{avg}}{|\bar{u}_s|} \approx 8.99$.

Figure 10. The effect of periodic bias flow with increasing grazing flow speed.

flow at $M_{avg} = 0.3$, the ratio of bias flow velocity to grazing flow speed should be $\frac{v_{avg}}{|\bar{u}_s|} < 5$. Consequently a periodic bias flow velocity of $|\bar{u}_s| > 20.6$ m/s needs to be applied. This poses a high energy requirement on the actuation source. While leakage of the bias flow actuation into the duct is not considered in this study, negative effects on the damping performance are expected and a trade-off analysis between the additionally induced noise and the enhanced damping needs to be conducted. Therefore, the actuation frequency should be preferably chosen in a way, that the propagation in the main duct is minimized. Taking into account all effects and tuning the components of the system properly, constitutes a challenge to the liner design.

VII. Conclusion and Outlook

Similar to a constant bias flow, periodic bias flow, induced by means of acoustic actuation, can be used to enhance the damping capabilities of lined surfaces over various operating conditions. Thereby, the amplitude of the periodic bias flow can be adapted to keep the resistance of the lined surface in a value range, where high damping is ensured. The Zero Mass Flow concept obtains broad band dissipation over a comparably large frequency range. The derived optimization process proves to be a viable tool in the design of acoustic liners. The predicted damping characteristics show good agreement to measurements. For combined periodic bias flow and grazing flow, the periodic bias flow is suppressed. This might pose a problem in the realization of Zero Mass Flow Liners for high mach number grazing flows, since a large amount of energy is necessary to achieve an effect. Hence, the periodic bias flow can be used to approximate the desired resistance values

This is the author's version (post-print) of the work that was accepted for publication in the proceedings of the 28th AIAA/CEAS Aeroacoustics Conference held in Southampton, United Kingdom, June 2022.
The final version was published in the proceedings of the conference as paper No. 2022-2820.
https://arc.aiaa.org/doi/abs/10.2514/6.2022-2820

in low Mach number regimes, while the liner should be optimized to working without periodic bias flow at high Mach numbers. Further research regarding the interaction of periodic bias flow and grazing flow needs to be conducted to gain further insights and refine the proposed model. The Zero Mass Flow concept might especially be useful in combination with multi cavity liners.

Appendix

A. The resistance of perforated plates under secondary high amplitude excitation

The periodic bias flow Strouhal number defined as $St_{p,d} = \frac{2\pi f_p d}{|\bar{u}_s|}$ is used as criterion to differentiate between the quasi-steady flow domain and the linear impedance regime. f_p represents the frequency of a primary excitation and d the diameter of the orifices. The primary excitation can be interpreted as the sound field to be damped by the ZML. $|\bar{u}_s|$ denotes the root mean squared (RMS) secondary particle velocity in the orifices of the facing sheet. $|\bar{u}_s|$ is induced by the acoustic actuator in the cavity of the liner causing the periodic bias flow through the perforations of the facing sheet. For small Strouhal numbers $St_{p,d} < 1$, the convective contributions to the resistance are large compared to the viscous effects and the change of the specific resistance at a frequency f_p of perforated plates due to secondary high amplitude excitation $Re\{\Delta\zeta_s\}$ can be approximated by using a quasi-steady assumption:[3]

$$Re\{\Delta\zeta_s\} = \frac{(1-\Phi^2)|\bar{u}_s|}{2c_0\Phi C_{d,nl}^2}, \tag{22}$$

where $C_{d,nl}$ describes the discharge coefficient approximated empirically, Φ represents the porosity of the facing sheet and c_0 describes the speed of sound in air. Conversely, for large Strouhal numbers $St_{p,d} \gg 1$ the convective contributions to the impedance can be neglected. Hence, the viscous contributions dominate and the impedance is only dependent on its geometric specifications. This regime is referred to as linear regime. Applying the quasi-steady approximation in the transitional domain between linear and quasi-steady flow regime may result in significant errors, when modelling the impedance of perforated plates. Muttalip et al.[23] extensively treated the impedance of micro-perforated plates in the transmission regime for single tone excitation. An empirical approximation to assess the effects of a secondary actuation on the impedance of perforated plates in transmission regime can be derived by analyzing the difference between the quasi-steady approximation and the measured resistance. The derivation is based on measurements of the impedance of perforated plates,[3,4] where the experimental setup and the evaluation method are described as well. We assume, that the change of resistance of the perforated sheet in the transitional domain can be approximated by Eq. (22) multiplied with an empirical factor Υ.

$$Re\{\Delta\zeta_s\} = \frac{(1-\Phi^2)|\bar{u}_s|}{2c_0\Phi C_{d,nl}^2} \cdot \Upsilon, \tag{23}$$

To obtain the deviation from the quasi-steady model, i.e. Υ, we divide the measured resistance values by Eq. (22) and yield:

$$\Upsilon = \frac{Re\{\Delta Z_s\} \cdot C_{d,nl}^2 \cdot 2\Phi}{(1-\Phi^2)\rho_0|\bar{u}_s|}, \tag{24}$$

where $Re\{\Delta Z_s\} = Re\{\Delta\zeta_s\} \cdot \rho_0 c_0$. Fig. 11 (a) and (b) show Υ, for two perforated plates, plotted against the inverse Strouhal number $1/St_{p,d} = \frac{|\bar{u}_s|}{2\pi f_p d}$. The dashed line represents the quasi-steady limit. As can be seen, with increasing $1/St_{p,d} > 1$, the change of resistance approaches Eq (22). For $0 < 1/St_{p,d} \leq 1$ considerable deviations from the quasi-steady approach are observed, that approximately follow the function $\Upsilon \approx 1 - \frac{f_p d}{|\bar{u}_s|}$, depicted as the dotted line. For the perforate depicted in Fig. 11 (a), a significantly different behavior of the resistance for $f_p << f_s$ (+ symbols) is observed and the impedance expresses a dependency on f_s. The deviate behavior is further discussed in Burgmayer et al.[3] For high $|\bar{u}_s|$, Υ approaches 1. For low $|\bar{u}_s|$, high f_p and large d, Υ can become negative as $\frac{f_p d}{|\bar{u}_s|} > 1$. Therefore, if $\Upsilon < 0$, we assume, that the resistance is independent of the particle velocity and $Re\{\Delta\zeta_s\} = 0$. The value of $\frac{f_p d}{|\bar{u}_s|} = 1$ corresponds to $1/St_{p,d} = \frac{1}{2\pi} \approx 0.16$, where effects due to high sound pressure amplitudes are negligible. Consequently, the semi empirical model to account for the change of resistance at a primary frequency f_p due to the secondary high amplitude actuation is written as:

This is the author's version (post-print) of the work that was accepted for publication in the proceedings of the 28th AIAA/CEAS Aeroacoustics Conference held in Southampton, United Kingdom, June 2022.
The final version was published in the proceedings of the conference as paper No. 2022-2820.
https://arc.aiaa.org/doi/abs/10.2514/6.2022-2820

$$Re\{\Delta\zeta_s\} = \frac{(1-\Phi^2)|\bar{u}_s|}{2c_0\Phi C_{d,nl}^2} \cdot (1 - \frac{f_p d}{|\bar{u}_s|}). \tag{25}$$

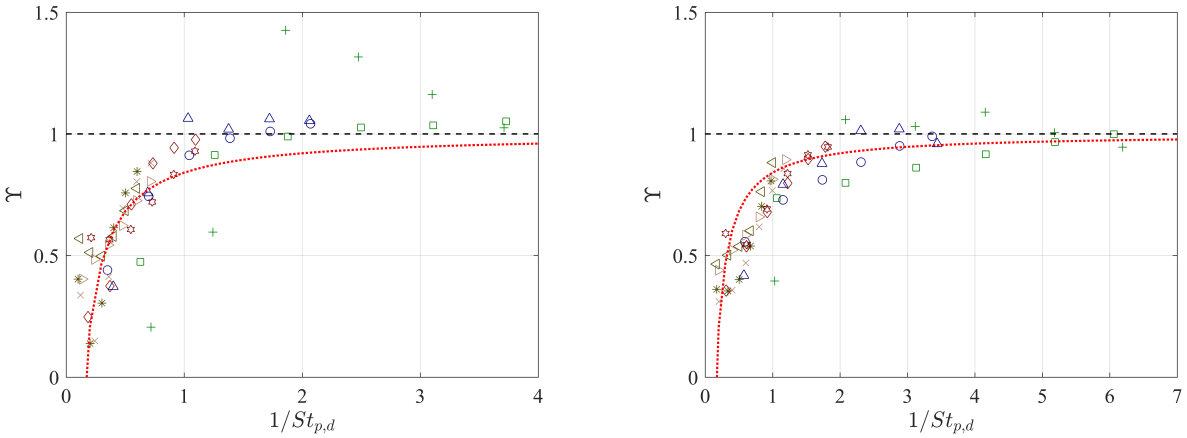

(a) $\Phi = 4.09$ %, $d = 2.5$ mm, $h = 1$ mm.

(b) $\Phi = 6.18$ %, $d = 1.5$ mm, $h = 1$ mm.

Figure 11. Deviation of resistance from quasi-steady solution in the transmission regime plotted against $1/St_{p,d}$. −−: Quasi-steady solution; ⋯: Approximation of the resistance in the transmission domain. Symbol reference for the measured resistance values:

	□	+	○	△	◊	▽	x	▷	∗	◁
f_p	255	255	459	459	867	867	1326	1326	1581	1581
f_s	331	943	331	943	331	943	331	943	331	943

Acknowledgements

This study is supported by the project ARTEM (Aircraft noise Reduction Technologies and related Environmental iMpact) which has received funding from the European Unions Horizon 2020 research and innovation programme under Grant No. 769 350.

References

[1]Heuwinkel, C., Enghardt, L., and Röhle, I., *Concept and Experimental Investigation of a Zero Mass Flow Liner*.

[2]Lahiri, C., Pardowitz, B., Bake, F., Röhle, I., and Enghardt, L., "Excitation of a Zero Mass Flow Liner for Acoustic Damping," *AIAA Journal*, Vol. 49, No. 3, 2011, pp. 513–519.

[3]Burgmayer, R., Bake, F., and Enghardt, L., "Effects of a secondary high amplitude stimulus on the impedance of perforated plates," *The Journal of the Acoustical Society of America*, Vol. 149, 05 2021, pp. 3406–3415.

[4]Burgmayer, R., Bake, F., and Enghardt, L., "Reduction of inertial end correction of perforated plates due to secondary high amplitude stimuli," *JASA Express Letters*, Vol. 2, No. 4, 2022, pp. 042801.

[5]Atalla, N. and Sgard, F., "Modeling of perforated plates and screens using rigid frame porous models," *Journal of Sound and Vibration*, 2007, pp. 195–208.

[6]Guess, A., "Calculation of perforated plate liner parameters from specified acoustic resistance and reactance," *Journal of Sound and Vibration*, Vol. 40, No. 1, 1975, pp. 119–137.

[7]Goldberg, D. E., *Genetic Algorithms in Search, Optimization and Machine Learning*, Addison-Wesley Longman Publishing Co., Inc., USA, 1st ed., 1989.

[8]Laly, Z., Atalla, N., and Meslioui, S.-A., "Acoustical modeling of micro-perforated panel at high sound pressure levels using equivalent fluid approach," *Journal of Sound Vibration*, Aug. 2018.

[9]Fok, V. A., "Theoretical study of the conductance of a circular hole, in a partition across a tube," *Proceedings of the USSR Academy of Sciences*, Vol. 31, 1941, pp. 875–878.

[10]Ingard, U., "Absorption Characteristics of Nonlinear Acoustic Resonators," *The Journal of the Acoustical Society of America*, Vol. 44, No. 4, 1968, pp. 1155–1156.

[11]Feder, E. and III, L. W. D., "Analytical and experimental studies for predicting noise attenuation in acoustically treated ducts for turbofan engines," 1969.

[12]Weng, C., Schulz, A., Ronneberger, D., Enghardt, L., and Bake, F., "Flow and Viscous Effects on Impedance Eduction," *AIAA Journal*, Vol. 56, No. 3, 2018, pp. 1118–113.

[13]Jones, M., Watson, W., and Parrott, T., *Benchmark Data for Evaluation of Aeroacoustic Propagation Codes with Grazing Flow*.

[14]Teixeira, F. and Chew, W., "A general approach to extend Berenger's absorbing boundary condition to anisotropic and dispersive media," *IEEE Transactions on Antennas and Propagation*, Vol. 46, No. 9, 1998, pp. 1386–1387.

[15]Oskooi, A. F., Zhang, L., Avniel, Y., and Johnson, S. G., "The failure of perfectly matched layers, and towards their redemption by adiabatic absorbers," *Opt. Express*, Vol. 16, No. 15, Jul 2008, pp. 11376–11392.

[16]Lahiri, C., *Acoustic performance of bias flow liners in gas turbine combustors*, Ph.D. thesis, Technical University Berlin, Berlin, Germany, 2013.

[17]Chung, J. Y., "Rejection of flow noise using a coherence function method," *The Journal of the Acoustical Society of America*, Vol. 62, No. 2, 1977, pp. 388–395.

[18]Dokumaci, E., "A note on transmission of sound in a wide pipe with mean flow and viscothermal attenuation," *Journal of Sound and Vibration*, Vol. 208, 1997, pp. 653–655.

[19]Goldman, A. L. and Panton, R. L., "Measurement of the acoustic impedance of an orifice under a turbulent boundary layer," *The Journal of the Acoustical Society of America*, Vol. 60, No. 6, 1976, pp. 1397–1405.

[20]Kooi, J. and Sarin, S., *An experimental study of the acoustic impedance of Helmholtz resonator arrays under a turbulent boundary layer*.

[21]Malmary, C., Carbonne, S., Auregan, Y., and Pagneux, V., *Acoustic impedance measurement with grazing flow*.

[22]Schulz, A., Weng, C., Bake, F., Enghardt, L., and Ronneberger, D., *Modeling of liner impedance with grazing shear flow using a new momentum transfer boundary condition*.

[23]Temiz, M. A., Tournadre, J., Arteaga, I. L., and Hirschberg, A., "Non-linear acoustic transfer impedance of micro-perforated plates with circular orifices," *Journal of Sound and Vibration*, 2016, pp. 418–428.

This is the author's version (post-print) of the work that was accepted for publication in the proceedings of the 28th AIAA/CEAS Aeroacoustics Conference held in Southampton, United Kingdom, June 2022.
The final version was published in the proceedings of the conference as paper No. 2022-2820.
https://arc.aiaa.org/doi/abs/10.2514/6.2022-2820